The Journal of Physiological Sciences 75 (2025) 100007

Contents lists available at ScienceDirect

The Journal of Physiological Sciences

journal homepage: www.editorialmanager.com/jphyss/default2.aspx

Circadian sleep–wake rhythm reversal in mice implanted with stomach cancer cell lines

Motohide Goto[a,1,*], Takashi Maruyama[b,1], Miki Nonaka[c,1], Yasuhito Uezono[c], Yoichi Ueta[b], Susumu Ueno[a]

[a] Department of Occupational Toxicology, Institute of Industrial Ecological Sciences, University of Occupational and Environmental Health, Japan
[b] Department of Physiology, School of Medicine, University of Occupational and Environmental Health, Japan
[c] Department of Pain Control Research, The Jikei University School of Medicine, Japan

ARTICLE INFO

Keywords:
Circadian rhythm
Cachexia
Day–night reversal
85As2
c-Fos
SCN

ABSTRACT

The present study explored the phenotype and behavioral characteristics of mice implanted with the 85As2 human stomach cancer cell lines. Generally, mice are nocturnal; they are active during the dark phase and resting in the light phase. However, mice implanted with 85As2 cells demonstrated diurnal patterns, showing activity in the light phase. The similar light–dark behavioral reversal was noted in mice implanted with other cancer cell lines, such as the HCT116 human colon cancer cell lines. Furthermore, 85As2 implanted mice revealed significant shortening of the free-running period under constant dark conditions. To explore the underlying physiological mechanisms of this circadian rhythm reversal, diurnal variations in the suprachiasmatic nucleus (SCN) were analyzed with observation of c-Fos expression. Interestingly, no significant difference was found in the SCN activity between the control and 85As2-implanted mice, demonstrating rhythm reversal. It is suggested that the lesion causing this rhythm reversal exists downstream of the SCN.

1. Background

Circadian rhythms are endogenous oscillations of biological processes that operate on a 24-h cycle, usually entrained to the daily environmental cycle. The sleep–wake cycle, which is central to these rhythms, is a critical regulator of metabolic, cognitive, and physiological functions in mammals [1]. Light influences the daily pattern of activity in mammals by entraining the circadian rhythms and acutely affecting activity; this phenomenon is known as masking [2]. Entrainment and masking allow organisms to match their behavior to the demands of a cyclic environment while maintaining a system that can respond to immediate environmental changes [3]. In diurnal species, light increases activity, whereas in nocturnal species, light induces sleep [4–7].

The suprachiasmatic nucleus (SCN) in the hypothalamus of the brain controls this diurnal rhythm [8]. A diverse range of pathological states, including metabolic disorders, neurodegenerative diseases, and cancers, have been linked to the disturbances in this cycle, which are often induced by external factors or genetic perturbations [9].

Interestingly, the oncology and circadian rhythm interface have recently garnered considerable research interest. Several studies have indicated that neoplasms can modulate the host's circadian rhythm via various mechanisms, such as the release of cytokines or direct interaction with the host's molecular clockwork [10]. Such observations raise the question of whether tumor growth could substantially impact the host's circadian regulation, potentially altering or even inverting the sleep–wake rhythm. Guided by this scientific premise, the current investigation examines the effects of tumor implantation into murine models on their endogenous sleep–wake cycle. Our study, leveraging insights from pioneering studies [10,11], aimed to elucidate the impact of tumor growth on circadian dysregulation and investigated whether tumor implantation can induce a reversal of the sleep–wake rhythms in mice.

A multifaceted syndrome characterized by significant weight loss, primarily from the loss of muscle and adipose tissues, is referred to as cancer cachexia. Cachexia is a type of malnutrition associated with chronic diseases, such as cancer, chronic heart failure, chronic renal failure, and autoimmune diseases, and is characterized by a decreased

* Correspondence to: Department of Occupational Toxicology, Institute of Industrial Ecological Sciences, University of Occupational and Environmental Health, 1–1 Iseigaoka, Yahatanishi-ku, Kitakyushu 807-8555, Japan.
E-mail address: motsu@med.uoeh-u.ac.jp (M. Goto).
[1] These authors equally contributed to this work.

https://doi.org/10.1016/j.jphyss.2025.100007
Received 30 July 2024; Received in revised form 20 January 2025; Accepted 24 January 2025

skeletal muscle mass. Weight loss is also a characteristic symptom of cancer cachexia, along with a reduced skeletal muscle mass [11]. This debilitating condition can seriously affect the treatment and have a substantial impact on a patient's quality of life. To understand the underlying mechanisms and to develop potential therapies, a robust animal model needs to be developed. Among the human stomach cancer cells, MKN45 emerged as a promising cell line owing to its capacity to induce body weight reduction, albeit with a 40 % incidence rate. Through meticulous culturing and subsequent xenografting, the 85As2 human stomach cancer cell line was derived from the MKN45 human stomach cancer cell line, which exhibited a more moderate malignancy as compared with 85As2. The 85As2 cancer cell line remarkably induced weight loss and peritoneal metastasis in rats, with an incidence rate of 100 % [12].

During breeding of mice implanted with the 85As2 cancer cells, we noted phenotypic alterations in their behavioral diurnal patterns. Consequently, we conducted observations and evaluations of the 85As2-implanted mice, highlighting these variations as a primary objective of our investigation. The present study aimed to examine the behavioral characteristics of 85As2-implanted mice and to observe the diurnal variations in the hypothalamus to elucidate the complex relationship between tumorigenesis and circadian homeostasis, potentially yielding remarkable insights for oncological and chronobiological research.

2. Methods

2.1. Animals

All experimental procedures were conducted according to the Guidelines for Animal Experiments and approved by the Committee for Ethics in Animal Experimentation of the University of Occupational and Environmental Health, Japan (approval number: AE18–010). These guidelines satisfy the ethical standards concerning experimental animals in Japan, as required by law. Seven-week-old male BALB/c AJcl-nu/nu mice were obtained from Clea-Japan (Tokyo, Japan). The animals were individually housed in cages under a 12:12-hour light–dark (LD) cycle (light on time: 7:00 am to 7:00 pm) at a temperature of 24 °C ± 1 °C and 55 % ± 5 % relative humidity, with access to water and standard laboratory food available. The animals were used for the experiments after 1 week of acclimatization. The home-cage activity was measured continuously for 2 weeks after implantation with LD cycle. The mice were then placed in constant darkness (DD) and finally returned to the LD cycle. The activity amount per hour was recorded and analyzed using an actogram.

2.2. Tumor implantation

The 85As2 cell line was derived from the human stomach cancer cell line MKN-45 via repeated implantation [12]. The cells were maintained at 37 °C in 95 % air and 5 % CO_2 with 95 % relative humidity in the RPMI-1640 medium (Nacalai Tesque, Inc., Kyoto, Japan) supplemented with 10 % fetal bovine serum (Invitrogen, Carlsbad, CA, USA), 100 IU mL^{-1} penicillin G sodium, and 100 μg mL^{-1} streptomycin sulfate (Nacalai Tesque, Inc.). Then, 85As2 cell suspension and implantation were employed to produce the implanted mice [12]. Mice anesthetized via inhalation of 3–3.5 % sevoflurane (Mylan, Osaka, Japan) were inoculated with subcutaneous injection (s.c.) of 1×10^5 and 1×10^6 85As2 cells per site (85As2-implanted mice) in the right and left flanks, respectively. Control (nontumor-bearing) mice were sham-inoculated with saline. The tumor volume was determined by measurement of the major and minor tumor axes with a caliper and extrapolation using the following equation: tumor volume (cm^3) = major axis (cm) × minor axis (cm) × minor axis (cm) × 1/2. The tumor volume, body weight, and food and water consumption were measured weekly.

2.3. Activity record

Using an animal movement analyzing system (ACTIMO-100N, SHINFACTORY, Fukuoka, Japan), comprising a rectangular enclosure (30 × 2 cm), with a side wall equipped with photo sensors at 2 cm intervals, spontaneous physical activity was measured. Each pair of photo sensors scanned any animal movement at 1 s intervals. After 2 weeks of 85As2 implantation, all mice were placed in individual cages. The counts of movement signals were conducted using the actogram. Locomotor activity and circadian cycles were scored using the Clock Lab program version 6.1.02 (Actimetrics Software, Wilmette, IL, USA). To measure the free-running period, the ClockLab program was used. We measured the mouse activity using the ClockLab analysis function, which tracks the locomotor activity and calculates the onset times based on the circadian cycle. The activity onsets were estimated using a template-matching algorithm. With the default setting, ClockLab searches for a 5-h period of inactivity followed by a 5-h period of high activity. The time of day that best approximates this pattern is considered the activity onset time.

During routine handling, we observed that the mouse activity temporarily increased on days when the weekly care routine was performed. This brief increase in activity could introduce artifacts that might affect the accuracy of the onset measurements. To prevent these artifacts from influencing our results, we excluded the data obtained from the days when the weekly care routine was conducted. This ensures that only consistent, undisturbed activity patterns are used for onset determination. By omitting these specific days from the analysis, more reliable and precise measurements of activity onset and phase shifts could be obtained.

2.4. c-Fos immunohistochemistry

The samples used to confirm c-Fos expression were taken at 8 weeks after transplantation when the day–night reversal of the activity phase was fixed entirely. The brains samples were collected at zeitgeber time 4 (ZT4) and ZT8 during the light phase and at ZT16 and ZT20 during the dark period (n = 4 for each time point). Additionally, the sampling during the dark phase at ZT16 and ZT20 was performed in complete darkness with only a red light on. The mice were deeply anesthetized via intraperitoneal administration of a combination of anesthetics. The mice were then transcardially perfused with 0.1 M phosphate buffer (PB; pH 7.4) containing heparin (1000 U/L), followed by 4 % paraformaldehyde (PFA) in 0.1 M PB. The brains were carefully removed and postfixed with 4 % PFA in 0.1 M PB for 48 h at 4 °C. The tissues were then cryoprotected in 20 % sucrose in 0.1 M PB for 48 h at 4 °C. Thereafter, the tissues were sliced into 30 μm sections using a microtome (Komatsu Electronics Co., Ltd., Hiratsuka, Japan). Brain slices, which contain the SCN in the hypothalamus, were collected from each brain sample. To evaluate c-Fos, one section was selected for the SCN at the same level of each brain; we prepared slices from the perfused and fixed mouse brains, focusing on the hypothalamus. From these, three slices containing the SCN were chosen. Then, all of the slices were immunohistochemically stained, the SCN region was delineated, and all slices were attached to the slides. The brain sections were incubated for 2 days at 4 °C with a rabbit polyclonal c-Fos antibody (ABE457; Sigma Aldrich, St. Louis, Mo, USA; 1:1000) in phosphate-buffered saline (PBS) containing 0.3 % Triton X-100 (PBST). After washing three times in 0.1 M PBS for 30 min in total, the sections were incubated overnight at 4 °C with a secondary antibody (Alexa Fluor 546 donkey anti-rabbit immunoglobulin G antibody; Molecular Probes, Eugene, OR, USA; 1:1000) in PBST. The sections were washed three times in 0.1 M PBS for a total of 30 min. The sections were then examined by fluorescence microscopy (VS120 Virtual Slide Microscope; OLYMPUS Corp., Tokyo, Japan) with an RFP filter (OLYMPUS Corp.). In the SCN, the c-Fos immunoreactive cells were counted for each captured image, and the c-Fos positive cells within the SCN were visually counted [13]. The cells

expressing c-Fos within this region were manually counted as c-Fos positive cells.

2.5. Diurnal activity after tumor removal

We investigated the changes in the actogram of the mice after removing the transplanted cancer cells. Following the 85As2 cancer cell transplantation, we observed a gradual advancement in the onset of the active phase in mice. At 5 weeks post-transplantation, once the light–dark activity rhythm had fully reversed and stabilized, we proceeded to remove the tumor. Under anesthesia, the mature tumor was carefully excised using precise surgical techniques, and the incision site was then sutured. Notably, the tumor showed no sign of adhesion or dissemination within the abdominal cavity, allowing for its complete removal in a single piece. Postoperatively, the mice quickly recovered from anesthesia and were housed in the same room as both the control mice and those that still retained tumors. The wounds of the mice fully healed within 2 weeks.

2.6. Statistical analysis

All data are presented as the mean ± standard error of mean. The data were analyzed for statistical significance via a paired *t*-test for determining differences between the two groups and using a one-way analysis of variance (ANOVA) or two-way ANOVA as necessary, followed by a post-hoc Bonferroni test for identifying the differences between multiple groups using GraphPad Prism version 5 (GraphPad Software Inc., San Diego, CA, USA). $P < 0.05$ was considered statistically significant.

3. Results

Change in the tumor size and body weight of 85As2-implanted mice The changes in the body weight of mice in the 85As2- implanted (n = 16) and control (n = 16) groups are demonstrated in Fig. 1A, and the changes in the tumor volume are shown in Fig. 1B. For the 85As2-implanted group, a cell suspension of the 85As2 human stomach cancer cell lines at 2×10^5 cells/mouse was subcutaneously implanted into the right abdomen after 1 week of acclimatization. Observations were made until 14 weeks after the start of rearing. The body weight of the 85As2-implanted mice was significantly reduced after a 4-week cancer cell implantation ($F\{29,233\} = 17.83$, $p < 0.01$). The size of the tumors in the 85As2-implanted group increased, resulting in cancer cachexia.

3.1. Diurnal variation in activity after tumor implantation

The actograms of the in the control (n = 8) and 85As2-implanted (n = 8) groups are presented in Fig. 2A and B, respectively. Moreover, the relative locomotive activities of the control and 85As2-implanted groups are shown in Fig. 2C and D, respectively. The tumor engraftment rate of the mice implanted with 2×10^6 cells/mouse was ≥ 90 %, as used in the cancer cachexia model, and all mice with tumors exhibited a diurnal activity pattern. Additionally, the tumor engraftment rate was approximately 60 % in mice implanted with 1/10 of this cell amount (2×10^5 cells/mouse), but all mice with tumors still exhibited a diurnal activity pattern.

The control group revealed a nocturnal activity pattern, resting during the light period and active during the dark period. A 24-h LD cycle in which the lights were turned on and off was maintained. However, in the 85As2-implanted group, the activity was initiated at 2 weeks after implantation; however, as the tumor grew, the activity start–end phase gradually advanced, and approximately 5 weeks after implantation, the activity phase reversed from that of the control group. It was confirmed that they entered a diurnal state, where they were active during the light period and rested during the dark period.

The onset activity time at 2 weeks (2 W), 5 weeks (5 W), and 8 weeks (8 W) after implantation was compared between the control and 85As2-implanted groups (Fig. 2E). The control group demonstrated that the onset of the active phase was absolutely during the nocturnal period (2 W = 16.86 ± 0.99, 5 W = 15.9 ± 1.11, 8 W = 19.7 ± 0.90), although the onset of the active phase of the 85As2-implanted group gradually advanced to the diurnal period after a 5-week cancer implantation (2 W = 17.66 ± 0.84, 5 W = 10.45 ± 0.55, 8 W = 9.23 ± 0.54: $F\{5210\} = 20.287$, $p < 0.01$ vs. control). The locomotor activity of the control and 85As2-implanted groups are shown in Fig. 2F (a, b, c).

Diurnal activity in the DD condition In the control group (n = 6), the actogram of the mice under the DD condition is demonstrated in Fig. 3A, and that of the 85As2-implanted group (n = 6) is shown in Fig. 3B. Both the control and 85As2-implanted groups exhibited a gradual advancement in the onset of the active phase. A 24-h shift advance was observed at 2–4 weeks after transplantation. The free-running period of the 85 As2-implanted mice under the DD condition was significantly shorter than that of the control group (control vs 85As2: 23.67 ± 0.003 vs 23.45 ± 0.012, p = 0.002). When the 85As2-implanted mice were placed back to the LD condition, the active phase was defined in response to light and the active phase remained reversed.

3.2. Actogram of mice implanted with other species causing cancer cachexia (HCT116)

The actogram of the mice implanted with other cancer cell lines (HCT116, human colorectal cancer cell lines) is illustrated in Fig. 4 (control group: n = 4, cancer-implanted group: n = 4). The measurement of the activity level was initiated at 2 weeks after implantation. The rate of the tumor volume increase in was slower in the HCT116-implanted group than in the 85As2-implanted group, and no change in

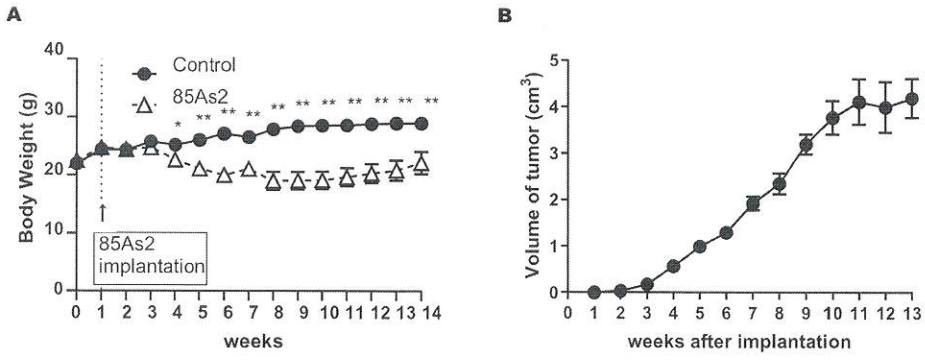

Fig. 1. A: Body weight of the control and 85As2-implanted mice. B: Increase in the size of the transplanted tumor. Body weight and volume of the tumor. The changes in the body weight of the control and 85As2-implanted groups (A). The body weight of the 85As2-implanted group was significantly decreased at 4 weeks after the cancer cell implantation ($F\{29,233\} = 17.83$, $p < 0.01$). A cell suspension of the 85As2 human stomach cancer cell lines at 2×10^5 cells/mouse was subcutaneously implanted into the right abdomen after 1 week of acclimatization. Observations were made until 14 weeks after the start of rearing (B). The tumor size in the 85As2-implanted group increased, leading to cancer cachexia. $^*p < 0.05$, $^{**}p < 0.01$.

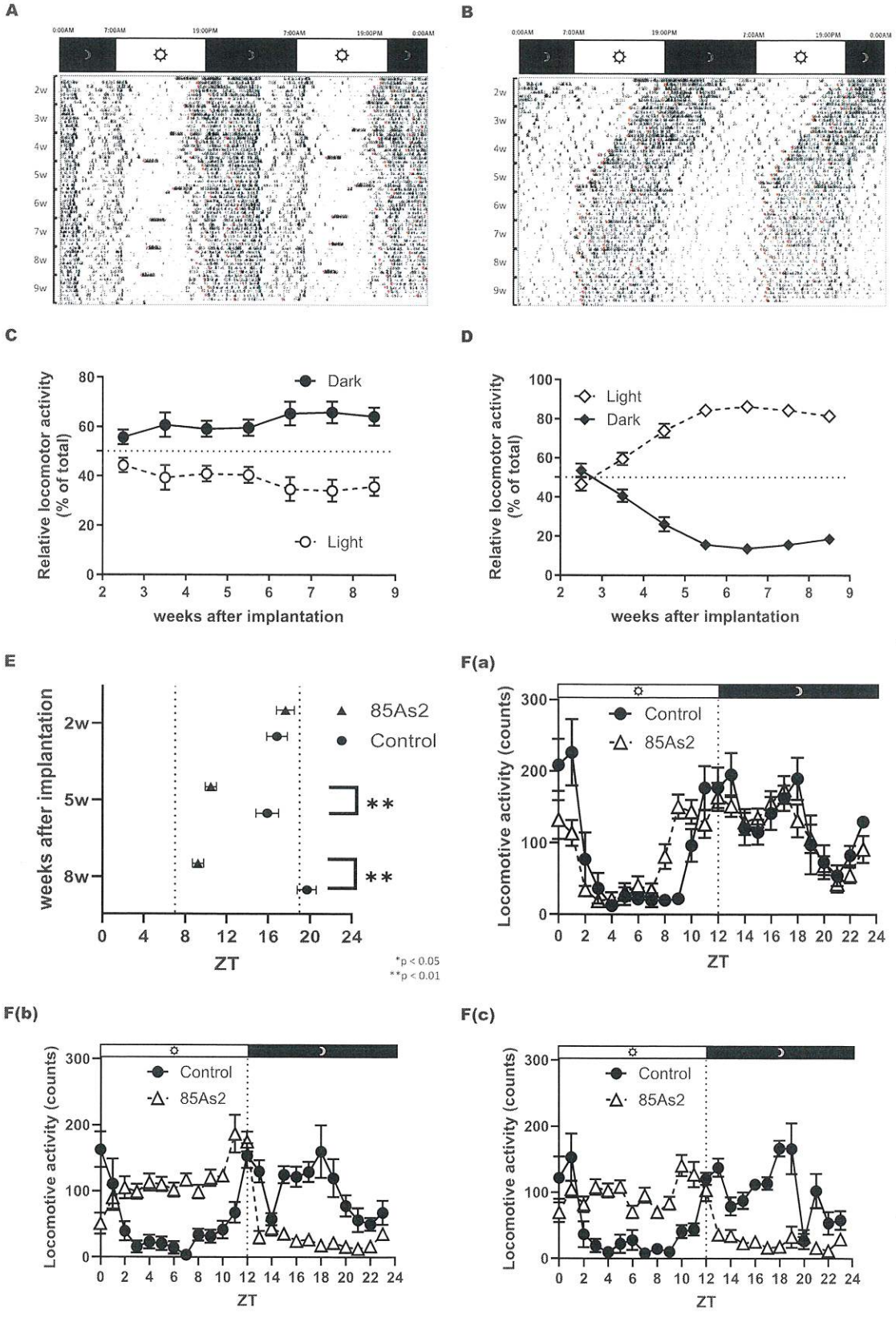

(caption on next page)

Fig. 2. A: Actogram of the control mice. B: Actogram of the 85As2-implanted mice. C: Relative locomotor activity of the control mice. D: Relative locomotor activity of the 85As2-implanted mice. E: Comparison of the onset of the activity phase between the control and 85As2-implanted mice. F: (a) Comparison of the locomotor activity between the control and 85As2-implanted mice (2 W); (b) comparison of the locomotor activity between the control and 85As2-implanted mice (5 W); and (c) comparison of the locomotor activity between the control and 85As2-implanted mice (8 W). The actogram and relative locomotor activity of the mice. The control group revealed a nocturnal activity pattern (resting during the light period and active during the dark period) (A, C). However, in the 85As2-implanted group, the measurement of activity was initiated at 2 weeks after implantation; however, as the tumor grew, the activity start–end phase gradually advanced, and approximately 5 weeks after implantation, the activity phase reversed from that of the control group (B, D). The onset of activity time at 2, 5, and 8 weeks after implantation was compared between the control and 85As2-implanted mice (E). The control group demonstrated that the onset time was absolutely a nocturnal period (2 W = 16.86 ± 0.99, 5 W = 15.9 ± 1.11, 8 W = 19.7 ± 0.90), although the onset time of the 85As2-implanted mice gradually advanced to the diurnal period at 5 weeks after the cancer cell implantation (2 W = 17.66 ± 0.84, 5 W = 10.45 ± 0.55, 8 W = 9.23 ± 0.54: F {5210} = 20.287, $p < 0.01$ vs. control). A comparison of hourly relative locomotive activity measurements between the control and 85As2-implanted mice (F) revealed the same pattern at 2 weeks after implantation in both groups (a). However, at 5 (b) and 8 (c) weeks after implantation, the 85As2-implanted group showed a diurnal pattern. Abbreviations: 2 W, 2 weeks; 5 W, 5 weeks; 8 W, 8 weeks.

the onset of the activity phase was noted for several weeks after implantation. As the tumor grew, the activity start–end phase gradually advanced, and finally, similar to the 85As2-implanted mice, at 11 weeks after implantation, the activity phase in the LD conditions reversed from that of the control group.

3.3. Observation of the SCN activity with c-Fos expression

Fluorescence observation of c-Fos protein expression in the SCN of the control and 85As2-implanted mice using immunohistochemical staining is shown in Fig. 5A and B. The brains of mouse containing SCN were sampled at four time points during the light (ZT4 and ZT8) and dark (ZT16 and ZT20) periods and c-Fos expression was analyzed using counts of c-Fos-positive cells. The c-Fos expression in the SCN considerably increased during the light period (ZT4: 97.0 ± 5.0 [control]/99.0 ± 4.58 [85As2], ZT8: 88.3 ± 5.87 [control]/98.25 ± 4.85 [85As2]) and decreased during the dark period (ZT16: 12.5 ± 2.50 [control]/10.0 ± 3.0 [85As2], ZT20: 7.0 ± 0.58 [control]/9.5 ± 1.0 [85As2]) both in the control and 85As2-implanted groups; however, no difference in c-Fos expression in the SCN was observed (F {7,14} = 87.777, $p < 0.01$) between the control and 85As2-implanted groups (Fig. 5B).

3.4. Diurnal activity after tumor removal

The actogram of the mice whose implanted tumors were removed at 5 weeks after implantation is demonstrated in Fig. 6 (control group: n = 4, 85As2-implanted group: n = 4, tumor-removed group: n = 4). After implanting the 85As2 cancer cells in mice, the onset of the active phase gradually advances, and the activity start–end pattern was completely reversed at 4 weeks after implantation. At 5 weeks after implantation, when the light-dark activity rhythm has been completely reversed and become fixed, the mature tumor was removed carefully by surgery under anesthesia. After tumor removal, the wound completely healed, the start–end phase of the activity was gradually delayed, and the mice that underwent tumor removal returned to their original nocturnal rhythm within a week.

4. Discussion

The pivotal discovery of this study is the pronounced impact of 85As2 cancer cell implantation on the circadian activity patterns of mice. A remarkable reversal from the intrinsic nocturnal behavior to a diurnal pattern was observed at approximately 2 weeks post -implantation, following tumor engraftment. Past experimental and clinical evidence indicates that malignant tumors can perturb the circadian rhythm of organisms [14,15]. However, no rodent model has offered consistent and reproducible observations of these rhythm changes due to the presence of malignancies. Even the development and validation of such a model alone is crucial for future detailed mechanistic studies of tumors and circadian rhythms.

Our initial hypothesis leaned toward altered SCN dynamics as a potential driver of behavior reversal post-tumor implantation, given the SCN's role as the central regulator of circadian rhythms post-tumor development. However, our experimental findings are in contrast to this hypothesis. Comparing the neuronal activity in the SCN, quantified by measuring the c-Fos expression, between the control mice and mice demonstrating a reversed light–dark rhythm post-tumor implantation revealed no significant variance. This consistency in the SCN reactivity pushes the focus toward potential alterations in neural circuits downstream of the SCN.

Although most rodents are nocturnal, notable exceptions also exist, such as the Nile grass rats with diurnal proclivities. A previous study involving Nile grass rats had reported unique light–dark and neural activity dynamics and indicated that the diurnal activity in SCN is similar between diurnal and nocturnal species, suggesting that their fundamental differences emerge from the mechanisms downstream of the SCN [16].

The hypothalamic subparaventricular zone (SPVZ), which extends dorsally and caudally from the SCN to the ventral edge of the hypothalamic paraventricular nucleus, may play an important role in the mediation of diurnality. The SPVZ, a significant target of the SCN, has efferent projections to some regions from the SCN in rodents, such as rats and hamsters. A previous study has revealed the possibility that the projections of the SCN and SPVZ are highly responsible for the diurnal and nocturnal phenotypes [17].

Tumor excision reinstated the original nocturnal behavioral patterns, further adding complexity to our findings. Our results also hinted toward tumor-derived humoral factors playing a role in the observed rhythmic disruption, a hypothesis that warrants further exploration and is supported by recent literature emphasizing the systemic influence of tumors [18].

Vinne et al. have reported that nocturnal mammals exhibit considerable plasticity in the circadian rhythm organization and may adopt a diurnal phenotype when facing energetic challenges [19]. They also highlighted that a neuronal mechanism, either downstream from or parallel with the central circadian pacemaker, i.e., the SCN, drives this shift. This behavioral phenotype is accompanied by a phase adjustment in the peripheral tissues, and a negative energy balance indeed promotes the diurnal response. The plastic transition from a nocturnal to a diurnal behavior observed in the cancer cell-implanted mice in our study appears similar. However, the mechanisms inducing this shift and its pathophysiology still need to be elucidated. In the present study, a nocturnal behavior was defined as occurring when 50–60 % or more of the total activity takes place during the dark phase, whereas a diurnal behavior was defined as occurring when 50–60 % or more of the total activity takes place during the light phase. Although the precise percentage-based definitions are rarely mentioned in literature, this approach aligns with the general findings of prior studies on rodent circadian rhythms [19].

This phenotypic flexibility allows nocturnal animals, such as mice, to shift their activity to the daytime in response to environmental challenges, including cold exposure, restricted food availability, or energetic stress. The diurnal shift observed in cancer-implanted mice may similarly reflect an adaptive behavioral change. Future studies

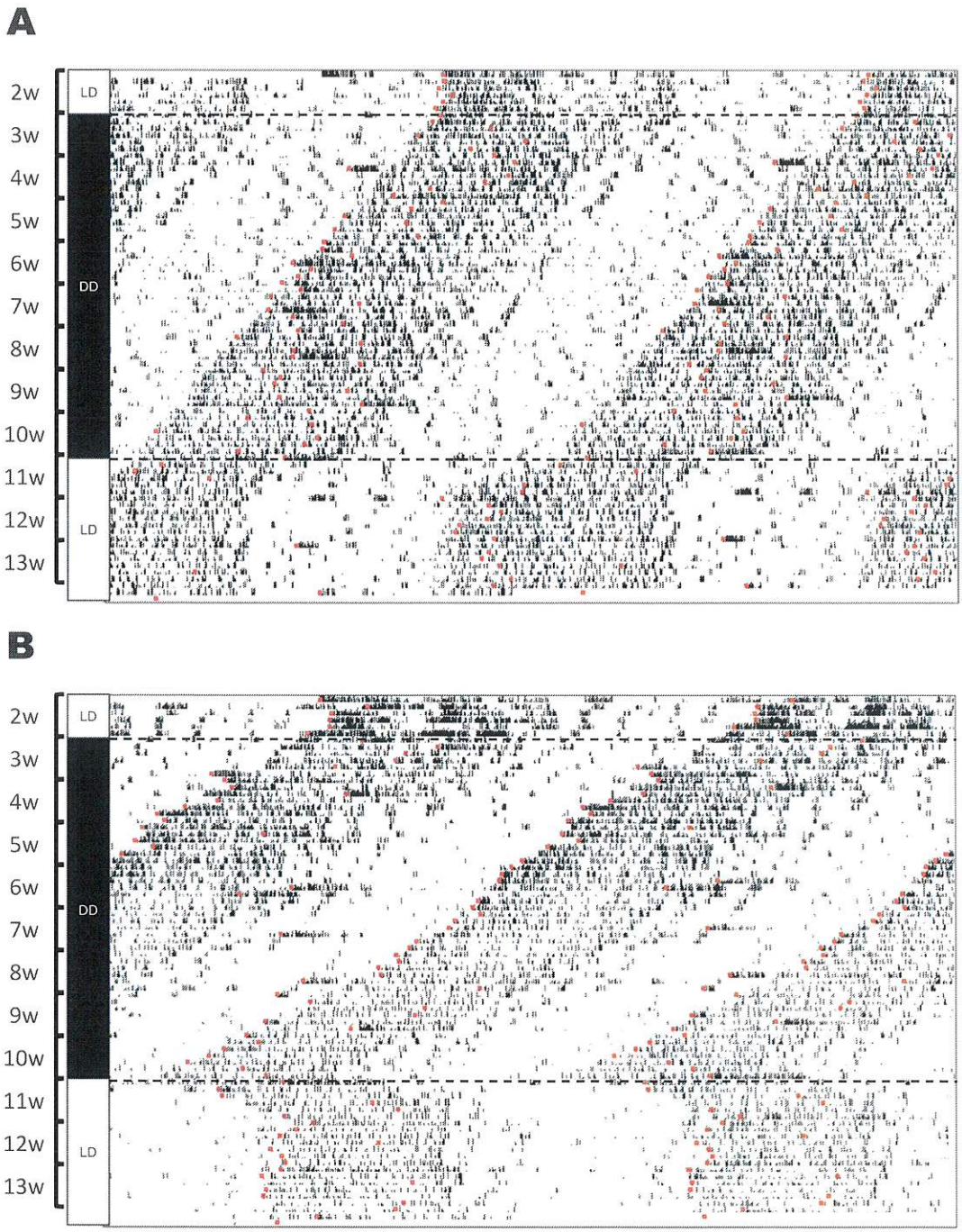

Fig. 3. A: Actogram of the control mice under the continuous dark environment. B: Actogram of the 85 As2-implanted mice under the continuous dark environment. An actogram of the control and 85As2-implanted mice under the continuous dark environment. The control mice exhibited a gradual advancement in the onset of the active phase (A). The 85As2-implanted mice also exhibited a gradual advancement in the onset of the active phase (B). The active phase of the 85As2-implanted mice gradually shifted from dark to light between 2 and 4 weeks after implantation and was almost reversed after 4 weeks. The free-running period of the 85As2-implanted mice under DD condition was significantly shorter than that of the control mice (control vs 85As2 mice: 23.67 ± 0.003 vs 23.45 ± 0.012, $p = 0.002$). When returned to LD conditions, the active phase was defined in response to light and remained reversed in the 85As2-implanted mice. Abbreviations: LD, light and dark; DD, continuous dark.

investigating the underlying mechanisms driving this plastic transition from a nocturnal to a diurnal behavior are needed. The present study, which elucidated the profound effects of tumor implantation on the circadian rhythms of mice, also showcased the intricacies of circadian regulation. The potential interplay between the tumors and neural pathways, considerably beyond the SCN, presents a promising avenue for future research. Further investigation into this relationship can provide invaluable insights into the nexus between oncogenesis and circadian rhythm dysregulation.

A limitation of the present study is that the c-Fos expression analysis was performed only at 8 weeks after the cancer cell transplantation, when the nocturnal to diurnal activity phase reversal was fully established. Although the final state of behavioral change was confirmed, we did not obtain a sample at the earlier stages, such as at 2 or 5 weeks

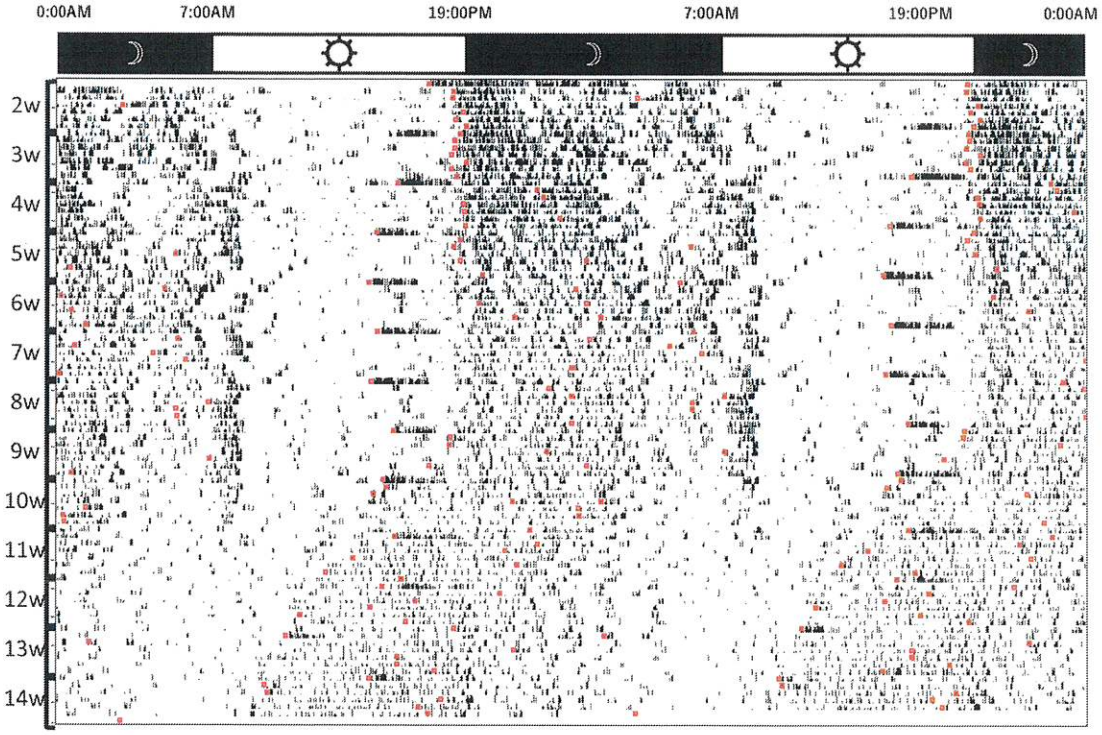

Fig. 4. An actogram of mice implanted with other species of cancer An actogram of the mice implanted with other species of cancer (HCT116 human colon cell lines). The measurement of the activity level was initiated at 2 weeks after implantation. The rate of the tumor volume increase was slower in the HCT116-implanted group than in the 85As2-implanted group, and no change in the activity phase was noted for several weeks after the implantation. As the tumor grew, the activity start–end phase gradually advanced, and finally, similar to the 85As2-implanted mice, at 11 weeks after the implantation, the activity phase in the light and dark conditions reversed from that of the control group.

after the transplantation, when the sleep–wake rhythm transition may have occurred. Sampling and analyzing the c-Fos expression during these periods could provide more detailed insights into the dynamic changes in the circadian rhythm mechanism. Hence, future studies should aim to perform such a time–course analysis to better understand the temporal effects of cancer cell implantation on circadian regulation. Moreover, we selected the images of c-Fos expression in the SCN from the best-condition samples for each time point. However, the shape and size of the SCN slightly vary between these images. This variant reflects the limitation of our experimental technique. Ideally, the shell and core subregions of the SCN should be counted separately. However, in the present study, the two subregions were analyzed together.

The assumption that rodents, including mice, are insensitive to red light has been prevalent, leading to its use during the dark phase in experimental settings [20]. In our study, we used red light with the lowest possible lux and performed sampling under conditions that minimized exposure to red light. The red light used for sampling was as dim as possible, with an intensity of < 0.4 Lx, and we ensured that the brain sampling procedure was completed as quickly as possible, within approximately 15 min. Therefore, we believe that the effect of red light

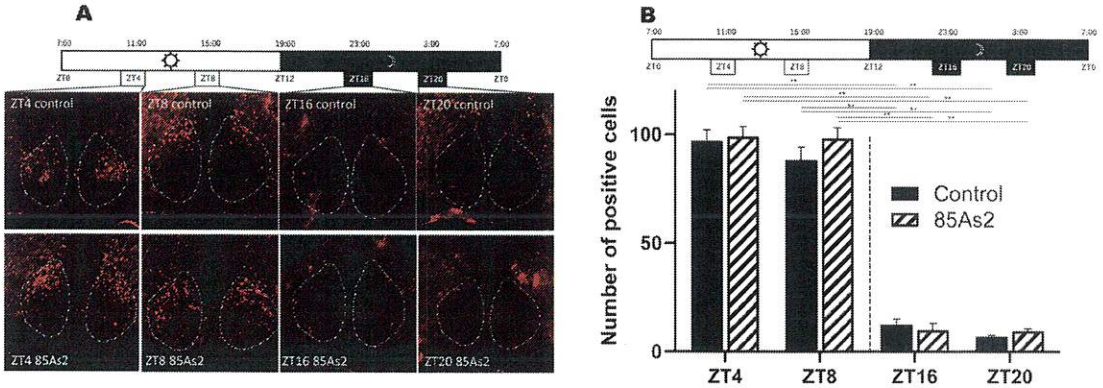

Fig. 5. Fig. 5A: c-Fos protein expression in the SCN. Fig. 5B: The counts of c-Fos positive cells in the SCN. The c-Fos expression in the SCN. Fluorescence observation of the c-Fos protein expression in the SCN of the control and 85As2-implanted mice using immunohistochemical staining (A). Mouse brains containing SCN were sampled at four time points during the light (ZT4 and ZT8) and dark (ZT16 and ZT20) periods, and c-Fos expression was analyzed by counting the c-Fos-positive cells. The c-Fos positive cell counts in the SCN considerably increased during the light period (ZT4: 97.0 ± 5.0 [control]/99.0 ± 4.58 [85As2], ZT8: 88.3 ± 5.87 [control]/98.25 ± 4.85 [85As2]) and decreased during the dark period (ZT16: 12.5 ± 2.50 [control]/10.0 ± 3.0 [85As2], ZT20: 7.0 ± 0.58 [control]/9.5 ± 1.0 [85As2]) both in the control and 85As2-implanted mice; however, no difference in c-Fos expression in the SCN ($F\{7,14\} = 87.777$, $p < 0.01$) was observed between the control and 85As2-implanted groups (B). Abbreviations: SCN, suprachiasmatic nucleus; ZT, zeitgeber time. $^{*}p < 0.05$, $^{**}p < 0.01$.

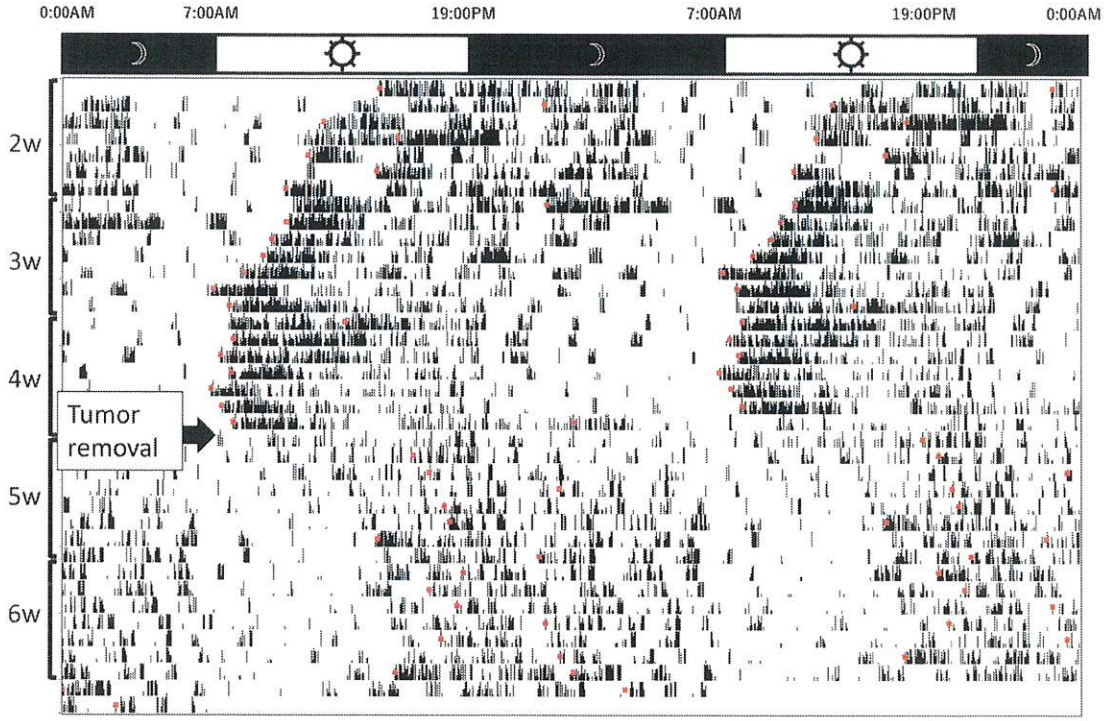

Fig. 6. An actogram of 85As2-implanted mice whose tumor was removed at 5 weeks after cancer implantation. The actogram of the mice whose implanted tumors were removed at 5 weeks after implantation. After the implantation of the 85As2 cancer cells in mice, the onset of the active phase gradually advances, and the activity start–end pattern was completely reversed at 4 weeks after implantation. At 5 weeks after implantation, when the light–dark activity rhythm was completely reversed and became fixed, the mature tumor was carefully removed by surgery under anesthesia. After tumor removal, the wound completely healed, and the start–end phase of the activity was gradually delayed, and the mice whose tumor was removed returned to their original nocturnal rhythm within a week.

on c-Fos expression in the SCN was minimized. However, it will be necessary to evaluate the SCN activity using other methods in the future.

5. Conclusion

The present study provides compelling evidence underscoring the effects of 85As2 cancer cell implantation on the circadian rhythm of mice, primarily manifesting as a reversal in their light–dark rhythms. This observed alteration in their circadian rhythm indicates that the changes in the light reactivity among mice has occurred. The neuronal activity within the SCN -the central regulator of circadian rhythm - remained unaltered between the tumor- implanted and control groups, despite these pronounced behavioral modifications. Furthermore, reversing this altered LD rhythm upon tumor excision reinforces the tumor's potential effects in modulating these rhythms.

These findings suggest a fundamental need for further exploration into the complex interactions between neoplastic growths and the nuanced mechanisms governing organismal circadian regulation. Although the underlying processes precipitating these observed effects are compelling, their complete characterization and neuronal mechanisms remain to be fully elucidated. Advancing this line of investigation is essential to delineate the specific mechanisms involved and drive potential breakthroughs in oncology and chronobiology.

Ethics approval

The experiments were approved by the University of Occupational and Environmental Health Japan Animal Care and Use Committee and conducted according to the committee's guidelines on animal care and use (permission number: AE18–018).

Funding

This work was partly supported by grants from the Japan Society for the Promotion of Science JSPS KAKENHI [grant numbers 17K01884, 20K18766, 21K11490 and 24K20188], grant from the Japan Agency for Medical Research and Development AMED [grant number JP22ck0106726] and the UOEH Research Grant for the Promotion of Occupational Health.

CRediT authorship contribution statement

Goto Motohide: Writing – original draft, Investigation, Funding acquisition, Formal analysis, Data curation. **Maruyama Takashi:** Writing – review & editing, Writing – original draft, Validation, Supervision, Investigation, Formal analysis, Data curation, Conceptualization. **Nonaka Miki:** Writing – review & editing. **Uezono Yasuhito:** Writing – review & editing. **Ueta Yoichi:** Writing – review & editing. **Ueno Susumu:** Validation, Supervision, Funding acquisition, Formal analysis, Data curation, Conceptualization, Writing – review & editing.

Availability of data and materials

The raw data supporting the study findings are available from the corresponding author upon reasonable request.

Declaration of Competing Interest

The authors declare that they have no known competing financial interests or personal relationships that could have appeared to influence the work reported in this paper.

Acknowledgements

The authors would like to thank Yuki Nonaka for providing experimental assistance. They would also like to thank Enago (www.enago.jp) for English language editing.

Supplementary Materials

Fig. 1 The SCN structure using DAPI staining. The representative images of c-Fos + DAPI, c-Fos expression, and DAPI staining are shown in a way to make c-Fos expression appear more straightforward, allowing the readers to visually understand the data. DAPI is a fluorescent stain that binds strongly to the adenine–thymine-rich regions in DNA. It is used extensively in fluorescence microscopy. Abbreviation: DAPI, 4′,6-diamidino-2-phenylindole.

Fig. 2 Transplantation of the 85As2 human stomach cancer cell line into mice. When the 85As2 human stomach cancer cells were transplanted subcutaneously into the abdominal cavity of the mice, the transplanted cells expanded and grew to a size of approximately 2 cm (A). When the skin was incised, a tumor was observed, but the cancer did not spread into the abdominal cavity or to the other organs (B). The removed tumor was a mass with a relatively clear boundary (C).

Appendix A. Supporting information

Supplementary data associated with this article can be found in the online version at doi:10.1016/j.jphyss.2025.100007.

References

[1] Hastings MH, Reddy AB, Maywood ES. A clockwork web: circadian timing in brain and periphery, in health and disease. Nat Rev Neurosci 2003;4:649–61. https://doi.org/10.1038/nrn1177.
[2] Redlin U. Neural basis and biological function of masking by light in mammals: suppression of melatonin and locomotor activity. Chrono Int 2001;18:737–58<https://DOI.ORG/10.1081/CBI-100107511>.
[3] Mrosovsky N, Thompson S. Negative and positive masking responses to light in retinal degenerate slow (rds/rds) mice during aging. Vis Res 2008;48:1270–3. https://doi.org/10.1016/j.visres.2008.02.016.
[4] Kumar V, Rani S. Light sensitivity of the photoperiodic response system in higher vertebrates: wavelength and intensity effects. Indian J Exp Biol 1999;37:1053–64.
[5] Peichl L. Diversity of mammalian photoreceptor properties: adaptations to habitat and lifestyle? Anat Rec Discov Mol Cell Evol Biol 2005;287:1001–12. https://doi.org/10.1002/ar.a.20262.
[6] Zubidat AE, Nelson RJ, Haim A. Photosensitivity to different light intensities in blind and sighted rodents. J Exp Biol 2009;212:3857–64. https://doi.org/10.1242/jeb.033969.
[7] Zubidat AE, Nelson RJ, Haim A. Differential effects of photophase irradiance on metabolic and urinary stress hormone concentrations in blind and sighted rodents. Chrono Int 2010;27:487–516. https://doi.org/10.3109/07420521003678577.
[8] Rosenwasser AM, Turek FW. Neurobiology of circadian rhythm regulation. Sleep Med Clin 2015;10:403–12. https://doi.org/10.1016/j.jsmc.2015.08.003.
[9] Wright KP, Drake AL, Frey DJ, Fleshner M, Desouza CA, Gronfier C, et al. Influence of sleep deprivation and circadian misalignment on cortisol, inflammatory markers, and cytokine balance. Brain Behav Immun 2015;47:24–34. https://doi.org/10.1016/j.bbi.2015.01.004.
[10] Logan RW, Sarkar DK. Circadian nature of immune function. Mol Cell Endocrinol 2012;349:82–90. https://doi.org/10.1016/j.mce.2011.06.039.
[11] Argilés JM, Busquets S, Stemmler B, López-Soriano FJ. Cancer cachexia: understanding the molecular basis. Nat Rev Cancer 2014;14:754–62. https://doi.org/10.1038/nrc3829.
[12] Terawaki K, Sawada Y, Kashiwase Y, Hashimoto H, Yoshimura M, Suzuki M, et al. New cancer cachexia rat model generated by implantation of a peritoneal dissemination-derived human stomach cancer cell line. Am J Physiol Endocrinol Metab 2014;306:E373–87. https://doi.org/10.1152/ajpendo.00116.2013.
[13] Motojima Y, Nishimura H, Ueno H, Sonoda S, Nishimura K, Tanaka K, et al. Role of Trpv1 and Trpv4 in surgical incision-induced tissue swelling and Fos-like immunoreactivity in the central nervous system of mice. Neurosci Lett 2018;678:76–82. https://doi.org/10.1016/j.neulet.2018.05.001.
[14] Sapolsky Sephton SE, Kraemer RM, Spiegel HC. D. Diurnal cortisol rhythm as a predictor of breast cancer survival. J Natl Cancer Inst 2000;92:994–1000. https://doi.org/10.1093/jnci/92.12.994.
[15] Relógio A, Thomas P, Medina-Pérez P, Reischl S, Bervoets S, Gloc E, et al. Ras-mediated deregulation of the circadian clock in cancer. PLOS Genet 2014;10:e1004338. https://doi.org/10.1371/journal.pgen.1004338.
[16] Smale L, Lee T, Nunez AA. Mammalian diurnality: some facts and gaps. J Biol Rhythms 2003;18:356–66. https://doi.org/10.1177/0748730403256651.
[17] Schwartz MD, Urbanski HF, Nunez AA, Smale L. Projections of the suprachiasmatic nucleus and ventral subparaventricular zone in the Nile grass rat (Arvicanthis niloticus). Brain Res 2011;1367:146–61. https://doi.org/10.1016/j.brainres.2010.10.058.
[18] Savvidis C, Koutsilieris M. Circadian rhythm disruption in cancer biology. Mol Med 2012;18:1249–60. https://doi.org/10.2119/molmed.2012.00077.
[19] van der Vinne V, Riede SJ, Gorter JA, Eijer WG, Sellix MT, Menaker M, et al. Cold and hunger induce diurnality in a nocturnal mammal. Proc Natl Acad Sci USA 2014;111:15256–60. https://doi.org/10.1073/pnas.1413135111.
[20] Nikbakht N, Diamond ME. Conserved visual capacity of rats under red light. eLife 2021;10:e66429. https://doi.org/10.7554/eLife.66429.